Energy Transfer From Antenna Ligand to Europium(III) Followed Using Ultrafast Optical and X-ray Spectroscopy

Michael W. Mara,[1,2] David S. Tatum,[1] Anne-Marie March,[3] Gilles Doumy,[3] Evan G. Moore [4] Kenneth N. Raymond[1,]*

[1]Department of Chemistry, University of California, Berkeley, California 94720, United States

[2]Chemical Sciences Division, Lawrence Berkeley National Laboratory, Berkeley, California 94720, United States

[3]Chemical Sciences and Engineering, Argonne National Laboratory, Lemont, Illinois 60439, United States

[4]School of Chemistry and Molecular Biosciences, University of Queensland, Brisbane, QLD 4072, Australia

*Corresponding Author: Raymond@socrates.berkeley.edu

Abstract

A series of highly luminescent europium(III) complexes which exhibit photoluminescence from the Eu(III) center following energy transfer from the UV absorbing organic sensitizer have been investigated using a combination of ultrafast optical transient absorption and Eu L3 X-ray transient absorption techniques. We have previously demonstrated that the latter can be used as a signature of 4f-4f excitation responsible for the photoluminescence in these Eu(III) coordination complexes, but the long timescale of the earlier measurements did not allow direct observation of the ligand-to-metal energy transfer step, preventing a determination of the sensitization mechanism. Here, we provide the first direct experimental verification that Dexter electron exchange from the ligand triplet state is the dominant energy transfer mechanism in these photoluminescent systems. Moreover, the optical transient absorption results obtained herein imply that energy transfer for all three compounds has near unity yield, regardless of differences in the sensitization efficiencies, suggesting that the variations in the sensitization efficiencies are determined almost entirely by differences in the ligand-centered intersystem crossing rates. The implications for the rational design of more effective photoluminescent lanthanide complexes are discussed.

Introduction

Luminescent materials are used in a wide range of scientific and industrial applications, including lighting and display screens,[1-2] lasers and fiber amplifiers,[3-5] and as biomedical dyes for imaging and fluoroimmunoassays.[6-17] Trivalent lanthanides have garnered particular interest in luminescence applications partly due to their sharp emission lines in the visible/near-IR and their long luminescence lifetimes, which are a product of 4f-4f transitions specific to each lanthanide (Figure 1a). These lanthanide transitions are almost entirely metal centered due to large spin-orbit coupling and very weak interaction with the ligand field. However, since the 4f-4f transitions are highly forbidden, and consequently direct 4f excitation is very weak, bright photoluminescent lanthanide complexes instead rely on indirect excitation utilizing the “antenna” effect, where a sensitizer (typically an organic ligand or a photoactive transition metal complex[18-21]) absorbs incident photons, leading to excitation of the lanthanide center by energy transfer.[7, 15, 22-28] A high efficiency Tb(III) complex developed as part of our research program is now used in several commercial assays,[29-32] and Eu(III)

complexes based on a different ligand system also now show similar high efficiency.[7, 22-23, 33-37] The overall quantum efficiency depends directly on the energy transfer efficiency, and hence determination of the energy transfer mechanism is of fundamental importance. Despite developments in the theoretical understanding of lanthanide systems,[38-44] experimentally monitoring energy transfer in photoluminescent lanthanide systems remains difficult, largely due to the absence of suitable experimental methods for directly probing the non-emissive lanthanide 4f excited states, which inhibits the rational design of highly efficient lanthanide-based fluorophores.

Generally, the two main energy transfer mechanisms which are applicable for lanthanide based systems are Förster resonant energy transfer[45] and Dexter electron exchange.[46] Förster transfer involves through-space resonant Coulombic interactions between the sensitizer and the lanthanide and, at lowest order, occurs when the transitions in the sensitizer and the lanthanide are both dipole-allowed. Instead, Dexter transfer is driven by through-bond electron exchange and requires a change in the spin multiplicity of both the sensitizer and lanthanide. Following these rules, and in accordance with detailed theoretical modelling, it can be expected that Förster transfer occurs from the ligand singlet state and Dexter transfer from the ligand triplet state,[47] with each transfer mechanism populating different excited 4f accepting states depending on the respective energies of the sensitizer ligand (Figure 1b). More recently, several authors have demonstrated singlet energy transfer may also occur from intraligand charge transfer (ILCT) states, where organic ligands with electronically conjugated donors and acceptors feature lower energy (near-UV to visible) ILCT states that can directly access 4f excited states similar to those accessed by Dexter exchange;[48-58] however, we have no spectral evidence or reason to expect that ILCT states are operative in the complexes reported here. Since Förster and Dexter transfer each have different energetic requirements to optimize the quantum efficiency, the dominant mechanism must be identified in order to enable rational design of more effective luminescent lanthanide complexes. Several studies have demonstrated that energy transfer most often occurs via the Dexter exchange mechanism from the ligand triplet state (as inferred by the agreement of calculated and observed transfer rates),[47, 59-64] but to the best of our knowledge, the mechanism of energy transfer for a photoluminescent lanthanide complex has not yet been directly demonstrated experimentally.

In order to elucidate the dominant energy transfer mechanism, the evolution of both the antenna and lanthanide excited states must be monitored following photoexcitation. In the former case, optical transient absorption (OTA) spectroscopy has proven to be effective in following the dynamics of the antenna, particularly when the antenna is an organic ligand that exhibits strong transient absorption features following photoexcitation.[23, 65-67] However, the lack of a strong OTA feature for the lanthanide center renders probing the metal center more difficult. Instead, X-ray transient absorption (XTA) can be employed as a direct probe of the lanthanide 4f states, as we have demonstrated previously.[68] By combining ultrafast optical and X-ray methods, we are able to determine which ligand excited state transfers energy to the metal center, and thereby confirm the energy transfer mechanism. In this study, we have focused on three europium(III) coordination complexes based on the 1-hydroxypyridin-2-one (1,2-HOPO) chromophore, as shown in the inset of Figure 2. These complexes have a minimized sensitizer-to-metal distance, with the 1,2-HOPO sensitizer being directly bound to the metal cation, which should allow for efficient energy transfer by both Förster and Dexter mechanisms. However, the selected complexes exhibit large variations in the overall quantum yield despite only minor differences in the chemical structure of the connecting ligand backbones. As a result, these

complexes have proven to be ideal for probing both the dominant energy transfer mechanism in typical antenna-based luminescence devices and for understanding the source of variation in sensitization efficiency and quantum yield.

Experimental

Sample Preparation and Luminesence Efficiency Measurements.

The organic ligands used for each complex are shown in Figure 2. Each Eu(III) complex adopts an overall ML_2 structure, wherein each of the two tetradentate ligands bind to the metal center via each of the four bidentate 1,2-HOPO chromophores (shown in green). As shown, the ligands differ only in the backbone substituent which connects the pair of 1,2-HOPO chromophores, yet these structural modifications result in significant changes in the luminescence properties of the corresponding Eu(III) complexes. All samples were prepared according to previously published methods, and sample integrity was verified by ESI-HRMS (Supporting Information).[33, 54, 68] Since X-ray absorption measurements require larger concentrations than optical measurements, methanol was used as the solvent rather than aqueous formulations for improved sample solubility.

The relevant photophysical parameters measured in methanolic solution for these complexes are shown in Table 1, and representative absorption and emission (which derive primarily from $^5D_0 \rightarrow {}^7F_J$, J = 1 – 4, in Eu(III) systems) spectra are shown in Figure 2. The overall quantum yield after 350 nm excitation was determined by the optically dilute method in comparison to quinine sulfate in 0.05 M H_2SO_4 as a well-established quantum yield reference (0.508, see Supporting Information). The metal-centered luminescence lifetimes were measured by monitoring the $^5D_0 \rightarrow {}^7F_2$ emission band at 612 nm following excitation at 350 nm. The instrument used for these measurements has been described elsewhere.[33] The remainder of the photophysical parameters in Table 1 were determined according to the methods outlined by Werts and Verhoeven,[69] which we briefly summarize. Specifically, there are two relevant efficiencies which dictate the total luminescence quantum yield: the efficiency of sensitizing the metal center and the efficiency of metal-centered radiative decay. Therefore, the total emission quantum yield Φ_{tot} can be defined as:

$$\Phi_{\mathrm{tot}} = \eta_{sens} * \Phi_{Eu} \qquad [1]$$

where η_{sens} and Φ_{Eu} are the efficiencies of sensitization and radiative decay, respectively. Normally, uncoupling $\eta_{sens}$and Φ_{Eu} would be problematic. However, the $^5D_0 \rightarrow {}^7F_1$ emission band for Eu(III) is purely magnetic dipole allowed, and it is the only $^5D_0 \rightarrow {}^7F_J$ transition with any magnetic dipole contribution. Since magnetic dipole transitions in lanthanide ions are practically independent of the ion's surroundings, the $^5D_0 \rightarrow {}^7F_1$ transition can be used as an internal standard to determine Φ_{Eu}, and by extension η_{sens} once Φ_{tot} is determined experimentally. The efficiency of radiative decay (Φ_{Eu}) is determined using the observed emission lifetime, τ_{obs}, and the radiative and non-radiative rate constants k_{rad} and k_{nr}:

$$\Phi_{Eu} = \frac{k_{rad}}{k_{rad} + k_{nr}} = \tau_{obs} * k_{rad} \qquad [2]$$

The only remaining unknown is k_{rad}, which can be evaluated as

$$k_{rad} = A_{MD,0} n^3 \frac{I_{tot}}{I_{MD}} \quad [3]$$

where I_{tot} is the integrated emission intensity over all of the $^5D_0 \rightarrow {}^7F_J$ transitions, and I_{MD} is the integrated intensity of the $^5D_0 \rightarrow {}^7F_1$ transition (measured from 580 – 600 nm). $A_{MD,0}$ represents the spontaneous emission probability of the $^5D_0 \rightarrow {}^7F_1$ transition, with a value of 14.65 s^{-1} *in vacuo*.[69-70] Solving for k_{rad} then enables us to determine Φ_{Eu}, and finally η_{sens}.

Optical Transient Absorption Measurements

Femtosecond transient absorption measurements were performed using an amplified laser system (Spitfire ACE, Spectra Physics) as the excitation source, delivering ca. 100 fs 800 nm laser pulses at a 1 kHz repetition rate. Approximately 0.1 mJ of this output was attenuated and focused onto a 3 mm CaF_2 window to generate a white light continuum probe pulse in the visible region from ca. 350 to 650 nm. The remainder of the laser fundamental was coupled to an OPA system (Topas Prime, Light Conversion) delivering femtosecond excitation pulses at 340 nm, and the pump pulse polarization was set to the magic angle with respect to the probe using a Glan-Taylor polarizer (GT10, Thorlabs). The absorbance of samples was approximately 0.6 over the 2 mm path length cell used, and samples were continuously stirred mechanically. The instrument response function (IRF) had a full width at half maximum (FWHM) of approximately 200 fs, as measured experimentally by a Gaussian fit to the scattered laser excitation profile, and all femtosecond spectra were corrected for the chirp of the probe pulses. For sub-nanosecond transient absorption measurements, a white light continuum from ca. 380 to 900 nm was generated using a pulsed Nd:YAG based Leukos-STM super continuum light source, the timing of which was controlled electronically using the sync out of the amplified laser system. The instrument response function (IRF) for this setup was ca. 100 ps. The resulting time traces were analyzed globally using GloTarAn and the R package TIMP.[71]

X-ray Transient Absorption Measurements

Transient X-ray absorption spectra were collected at the Advanced Photon Source on beamline 7-ID,[72] using the MHz-repetition-rate pump-probe, liquid-jet endstation.[73] A recently installed, cryo-cooled, double-crystal, Si(111) monochromator produced X-rays with ~0.8 eV bandwidth around a central photon energy of 7 keV. The energy of the X-rays was calibrated using an Fe foil and the average X-ray flux at the sample was measured to be ~4 x 10^{12} photons/second using an ion chamber. The synchrotron ran in the standard 24-bunch operating mode, producing X-ray pulses with an 80 ps duration (FWHM) at 6.52 MHz repetition rate. The laser (355 nm wavelength, 10 ps pulse duration, Duetto, Lumentum) was synchronized to the storage ring and operated at 1.3 MHz so that laser pulses overlapped every 5th X-ray pulse. At this repetition rate, the X-ray pulses overlapped with the laser are from each of the 24 electron bunches circulating the ring, allowing us to use the ungated ion chamber measurement as an incident X-ray flux monitor for the pump-probe measurements. The laser pulse fluence was ~12 mJ/cm^2 and spot size at the sample ~20 um FWHM.

The sample was circulated by a HPLC pump through a 200 µm diameter quartz nozzle that produced a cylindrical liquid jet. The flow rate was set to 50 mL/min to ensure a jet speed of ~25 m/s to fully refresh the sample volume between laser shots. The X-rays were focused onto the jet to a spot size of 5 µm (H) x 3 µm (V) FWHM using Kirkpatrick-Baez mirrors. The laser beam crossed the X-ray beam with a small (~5 degrees) angle and was spatially overlapped with the X-rays at the jet position using a 50 µm diameter pinhole. Temporal

overlap between laser and X-rays was performed using an MSM detector (Hamamatsu) to ~10 ps precision and then spatial and temporal overlap was optimized using the $[Fe(bpy)_3]^{2+}$/acetonitrile reference sample, which is known to have a prompt response.[74]

XAS spectra were collected in fluorescence mode at 90 and 270 degrees relative to the incident X-ray beam using 2 APD detectors (Oxford instruments). One operated in analog mode and was positioned closer to the jet so as to detect multiple fluorescence photons per shot. The signal was input in a MHz digital boxcar average (UHFLI, Zurich Instruments) to provide average signals for the X-ray pulses just preceding the laser-overlapped pulses (OFF) and the X-ray pulses overlapped with laser pulses (ON). The second detector was operated in photon counting mode and positioned opposite the first detector and farther from the jet so as to detect on average ~0.1 counts/shot. The signal was routed through a CFD and then sent into FPGA-based gating electronics that tallied counts for the OFF and ON bunches.

Results

Sensitization Efficiencies

A summary of relevant photophysical parameters measured for the three investigated complexes is given in Table 1, while absorption vs. total emission profiles for the europium complexes compared to quinine sulfate used to determine the overall photoluminescence quantum yields (Φ_{tot}) are shown in the Supporting Information. The general trends previously observed in η_{sens} for aqueous solutions are also found here; namely, that $[Eu\mathbf{3}_2]^-$ has a much lower sensitization efficiency than that observed for $[Eu\mathbf{1}_2]^-$ and $[Eu\mathbf{2}_2]^-$, both of which are comparable. In aqueous solution, $[Eu\mathbf{2}_2]^-$ has a lower Φ_{tot}, comparable to that of $[Eu\mathbf{3}_2]^-$, largely due to solvent quenching which lowers Φ_{Eu}. This was previously shown to be the result of solvent access to the metal center,[33] resulting in more rapid deactivation of the Eu 4*f** excited state. However, this was not observed in methanol, where Φ_{Eu} is roughly 0.5 for all complexes, suggesting less overall interaction between the solvent and the metal center in non-aqueous solution. Supporting the lack of significant solvent interactions in methanol, quantum yields were also collected in deuterated methanol and were found to be only slightly higher for all three Eu(III) complexes (Table 1). Comparing the observed lifetimes for all three samples in methanol and deuterated methanol gives an estimate of 0.5 units of methanol bound to the inner coordination sphere for all three samples, which we interpret as 0 units of methanol given the limitations of the empirical equation used and the presence of amide protons than can be exchanged for deuterons in deuterated methanol.[75]

Optical Transient Absorption

Transient absorption measurements utilizing an optical probe pulse were undertaken to analyze the excited state dynamics of the 1,2-HOPO ligand following UV excitation. Initial measurements utilized the Gd(III) analogs of the Eu(III) complexes, since energy transfer to Gd(III) cannot occur due to the lack of energetically accessible excited 4*f** states on the Gd(III) cation (Figure 1a). Nanosecond OTA spectra for $[Gd\mathbf{1}_2]^-$, $[Gd\mathbf{2}_2]^-$, and $[Gd\mathbf{3}_2]^-$ are shown in the Supporting Information, with each complex exhibiting a single exponential decay component with a time constant of ca. 150-200 ns, assigned to ligand triplet decay. The corresponding ultrafast OTA spectra, along with the evolution associated spectra (EAS) for each of the complexes are shown in Figure 3. For both $[Gd\mathbf{1}_2]^-$ and $[Gd\mathbf{2}_2]^-$, the initially observed spectra consist of an excited state absorption

(ESA) spectrum with a peak at *ca*. 375 nm and a second relatively broad ESA feature between 430-600 nm. These signals rapidly evolve to a long lived feature between 360-450 nm, with a peak at *ca*. 390 nm. The corresponding time resolved decay dynamics associated with these features clearly show the presence of two lifetime components: one on the picosecond timescale, which is assigned to local excited singlet state initially populated immediately after excitation, and the latter assigned to the corresponding triplet excited state which was fixed to the value obtained by nanosecond OTA measurements. Instead, for $[Gd\mathbf{3}_2]^-$, the initially observed OTA spectrum differs significantly, showing a more intense and blue shifted ESA feature between 350-510 nm, with a peak at *ca*. 385 nm, and a smaller shoulder at ca. 450 nm. This feature evolves into a longer lived signal with a much weaker intensity and less pronounced ESA features between 370-490 nm. Importantly, the corresponding decay dynamics for these OTA signals could not be satisfactorily fit to a biexponential decay model (see Supporting Information), and instead required three lifetime components to obtain a satisfactory fit, as summarized in Table 2. These differences point to significantly different electronically excited state structure for the 1,2-HOPO chromophore in the $[Gd\mathbf{3}_2]^-$ complex, potentially demonstrating a different excited-state singlet structure. Corresponding TD-DFT measurements (shown in Supporting Information) confirm that for the $[Eu\mathbf{1}_2]^-$ and $[Eu\mathbf{2}_2]^-$ complexes, the ligand backbone is isolated from involvement in the electronically excited state transitions by the $-CH_2-$ linkers, whereas for $[Eu\mathbf{3}_2]^-$, direct attachment of the aryl group to the 1,2-HOPO chromophore results in significant involvement of the ligand backbone to the lowest energy excited singlet states.

Subsequent ultrafast OTA spectra obtained for the $[Eu\mathbf{1}_2]^-$, $[Eu\mathbf{2}_2]^-$, and $[Eu\mathbf{3}_2]^-$ complexes, and the corresponding evolution associated spectra (EAS), are shown in Figure 4. The observed spectral features are essentially the same as those seen in the Gd(III) complexes, as expected, since it is the ligand based electronic transitions which are being probed. However, the time resolved decay dynamics evaluated by global fitting of the observed spectral features are considerably reduced, as summarized in Table 2. Most importantly, the longer lived ESA signals assigned to electronically excited triplet state of the 1,2-HOPO chromophore decays almost completely to the baseline over the available experimental time window (~2.7 ns). The substantial decrease in the excited state lifetimes can be related to the efficiency of energy transfer, and will be discussed in more detail below (see Discussion).

X-ray Transient Absorption

The ground-state Eu L3 X-ray absorption near edge spectra (XANES), which involve excitation of core $2p_{3/2}$ electrons either to bound unoccupied Eu orbitals or out of the atom completely (ie. past the Fermi level), are shown for the $[Eu\mathbf{2}_2]^-$ complex in Figure 5. The XANES spectra are dominated by broad, dipole-allowed 2p-5d transitions known as the white line, along with a weak pre-edge feature consisting of quadrupole-allowed 2p-4f transitions. In this case, the white line of $[Eu\mathbf{2}_2]^-$ is broadened due to the short 2p core hole lifetime such that the pre-edge feature is only visible in high energy resolution measurements. As a representative example, the XANES spectrum of photoexcited $[Eu\mathbf{2}_2]^-$, collected 5 ns after photoexcitation, is also shown in Figure 5. While the observed photoinduced changes are small, the difference spectrum shows a clear shift in the white line energy and intensity. No clear variation is observed at the pre-edge here, though this may be due to the strong overlap with the white line. Since no significant changes at the pre-edge feature were observed, the time-dependent dynamics of the Eu 4f states were instead monitored using the strongest feature in the XANES

spectrum, which in this case is the difference signal at 6.9815 keV. This feature corresponds to a shift in the white line, which was previously demonstrated to be sensitive to changes in the Eu 4f manifold as a result of 4f-5d Judd-Ofelt hybridization.[68] This orbital mixing effect is analogous to the 3d-4p mixing observed in the K-edge XAS spectra in most non-centrosymmetric 3d transition metals.[76-78]

As a representative example, kinetic traces of the XANES spectra for $[Eu\mathbf{2}_2]^-$ at 6.9815 keV are shown in Figure 6, and are well reproduced using a biexponential function, with a 1.4 ns time constant and a longer time constant that exceeds the 140 ns scan limit. The second time constant may reflect a longer lived Eu excited state, but it is also affected by the flow rate and pump laser spot size in this experiment. The first component reflects the timescale of excitation of the metal center, which almost perfectly matches the 1.4 ns time constant obtained for decay of the ligand centered excited triplet state obtained by OTA. Similar results were obtained for the $[Eu\mathbf{1}_2]^-$ and $[Eu\mathbf{3}_2]^-$ (Supporting Information). An overlay of the OTA and XANES kinetics is also shown in Figure 6, where the normalized XANES kinetic data is plotted with the observed OTA decay dynamics trace at 400 nm, which is dominated by the third spectral component (i.e., the ligand triplet state.) These two kinetic traces overlay extremely well, and the matching of these two kinetic processes unambiguously confirms that decay of the ligand triplet state leads directly to excitation of the Eu(III) center.

Discussion

Energy Transfer from Triplet State Is >99% Efficient For All Eu(III) Complexes

As demonstrated using OTA techniques, the most significant difference between the dynamics of the Eu(III) and Gd(III) complexes is the lifetime of the ligand centered triplet excited state, which decays orders of magnitude faster for the former (*vide supra*). The increased decay rates for the Eu(III) complexes can be attributed to faster depopulation of the triplet state via energy transfer to the Eu(III) ion, whereas this energy transfer is not possible for the analogous Gd(III) complexes. The ratio of these two rates can be used to determine the efficiency of energy transfer from the triplet state, under the assumption that the radiative and non-radiative decay rates of the triplet state for the Gd(III) complexes reflect those of the Eu(III) complexes in the absence of energy transfer, such that:

$$\eta_{ET} = 1 - \frac{k_{Gd}}{k_{Eu}} = 1 - \frac{\tau_{Eu}}{\tau_{Gd}} \qquad [1]$$

The resulting efficiencies are shown in Table 2. Most notably, each Eu(III) complex has an efficiency for energy transfer from the ligand triplet state to the metal of > 99%, despite the variations in sensitizer efficiency, η_{sens}, noted across the ligand series. The very high energy transfer efficiency can be rationalized by the direct bonding of the 1,2-HOPO chromophore to the metal center, minimizing the donor-acceptor distance and establishing strong wave function overlap for optimal energy transfer.

Dexter Transfer Is the Dominant Energy Transfer Mechanism For Eu(III)-HOPO Complexes

While the OTA measurements demonstrate the high efficiency of triplet state energy transfer, they do not explicitly demonstrate the dominant energy transfer mechanism, as a significant amount of Förster resonant energy transfer from the ligand singlet state could still be possible. However, the combination of the OTA and

XTA measurements clearly demonstrate which ligand state is responsible for excitation of the Eu(III) metal center, and hence which mechanism is dominant. The XANES difference spectra reported herein appear with a 1-2 ns time constant, with continued evolution occurring over 100's of nanoseconds or longer. Optical emission measurements have previously demonstrated that the emissive Eu(III) $^5D_0$ state is populated by the $^5D_1$ state on a timescale of 1-2 μs,[23] while direct population of the $^5D_0$ state is also possible at higher temperatures via the thermally-populated $^7F_1$ lower excited state.[79-80] Therefore, our measurements likely probe an admixture of the $^5D_1$ and $^5D_0$ states. If Dexter energy transfer from the ligand centered triplet state is the dominant mechanism, the XANES difference signal would be expected to grow in concurrently with decay of the ligand triplet state. For Förster transfer, a higher energy 4f state would be initially populated, followed by eventual decay to the $^5D_1$, which would manifest as a multiexponential growth in the XANES difference signal with the earliest component matching the ligand singlet state decay time. However, our XTA growth time is monexponential and matches the ligand triplet decay time, indicating that the Eu(III) center is excited primarily via the ligand centered triplet state. Considering the selection rules for energy transfer in these systems (*vide supra*), we conclude that Dexter mediated energy transfer is the dominant mechanism in these systems, with little to no Förster transfer occurring. To the best of our knowledge, this is the first time that the energy transfer mechanism has been explicitly demonstrated experimentally for organic lanthanide complexes. This mechanism is also likely dominant for the d-f bimetallic assemblies of Lazarides and Ward, as the photoexcited MLCT states there have ISC rates that will exceed those of the organic sensitizers used here.[18-21]

Energy Transfer Efficiency is Determined by the Intersystem Crossing Rate

Together, our results demonstrate that, for the family of 1,2-HOPO complexes investigated here, energy transfer occurs primarily through a Dexter electron exchange mechanism, which has near unity efficiency once the ligand triplet state is reached. Because the near unity energy transfer efficiency is observed for all three complexes despite variations in the sensitization efficiency across the ligand set, we conclude that the sensitization efficiency is instead dictated by ligand-centered processes leading to population of the ligand triplet state, specifically the competition between the rate of intersystem crossing and other ligand mediated singlet state decay pathways. Notably, the longest-lived component in the OTA spectrum of the $[Gd\mathbf{3}_2]^-$ complex exhibits a much weaker magnitude for the third EAS component compared to both $[Gd\mathbf{1}_2]^-$ and $[Gd\mathbf{2}_2]^-$ (Figure 3), consistent with a lower overall efficiency for the ISC process for ligand **3**. Less efficient ISC is also reflected by the much shorter decay times obtained for the initially populated singlet excited state of the $[Ln\mathbf{3}_2]^-$ complexes (and only very small differences between Ln = Gd *cf* Eu) when compared to $[Ln\mathbf{1}_2]$ and $[Ln\mathbf{2}_2]^-$, suggesting radiative and, more likely, non-radiative relaxation pathways of the singlet excited state are able to more efficiently compete with ISC, resulting in only a small population of the ligand triplet state in the $[Ln\mathbf{3}_2]^-$ complexes. In this case, the best method to optimize the sensitization efficiency in such complexes would be to facilitate more efficient population of the excited triplet state, either by improving intersystem crossing or inhibiting singlet decay back to the ground state.

Since each complex includes the same 1,2-HOPO chromophore and metal center, it is not readily apparent as to why the ISC efficiency should vary so significantly across the series. In a recent study, the results of TD-DFT calculations pointed to $[Eu\mathbf{3}_2]^-$ having a triplet state energy that is too low in energy to populate the $^5D_1$ Eu(III)

state, and therefore the authors concluded that sensitization must proceed by a different mechanism involving only the $^5D_0$ Eu(III) state.[81] However, the triplet state energies of these complexes have been shown experimentally to be equivalent to each other by recording the phosphorescent emission of the Gd(III) complexes at 77 K (Supporting Information).[33] Furthermore, all three Eu(III) complexes have measureable emission from the $^5D_1$ state, and there is no difference in the proportion of $^5D_1$ emission relative to the total $^5D_1$ and $^5D_0$ emission between these three complexes, which rules out any significant decrease in the triplet state energy or change in sensitization mechanism for $[Eu\mathbf{3}_2]^-$ relative to the other samples (Supporting Information). Instead, we note that for the $[Ln\mathbf{3}_2]^-$ complexes, the linkage between the 1,2-HOPO chromophores is shorter and includes conjugation of the aryl group across the ligand backbone that is not present for either the $[Ln\mathbf{1}_2]^-$ or $[Ln\mathbf{2}_2]^-$ complexes. We propose that the presence of this conjugated aryl linkage significantly alters the structure of the electronically excited singlet states, which is supported by our TD-DFT calculations and is also consistent with the significant differences in singlet excited state behavior we observe from the ultrafast OTA measurements. As a result of this difference, the efficiency of intersystem crossing in the $[Ln\mathbf{3}_2]^-$ complexes is considerably reduced, leading to a less efficient sensitization process overall. We continue to investigate the remarkable sensitivity of the intersystem crossing rates to small structural changes of the complexes, as such properties will profoundly affect the rational design of more effective luminescent lanthanide complexes.

Conclusions

We have utilized a combination of ultrafast optical transient absorption and time-resolved Eu L3 X-ray absorption spectroscopy to elucidate energy transfer by independently probing both the sensitizer ligand and lanthanide center. We demonstrate experimentally that the europium(III) excited 4f states are directly populated by Dexter electron exchange from the ligand triplet state, with essentially no Förster contribution from the ligand singlet state. We further demonstrate that the Dexter energy transfer has an extremely high efficiency (>99%), suggesting that the overall sensitization efficiency is likely dictated by competition between intersystem crossing and other excited singlet state decay pathways. It is clear that optimization of the sensitizer efficiency, and thus luminescence brightness, requires improving the intersystem crossing rate relative to nonradiative singlet state decay.

Supporting Information Available

Mass spectrometry data for $[Eu\mathbf{1}_2]^-$, $[Eu\mathbf{2}_2]^-$, and $[Eu\mathbf{3}_2]^-$. Total emission quantum yield measurements in methanol and deuterated methanol. Nanosecond transient absorption spectra for $[Gd\mathbf{1}_2]^-$, $[Gd\mathbf{2}_2]^-$, and $[Gd\mathbf{3}_2]^-$. XTA/OTA comparisons for $[Eu\mathbf{1}_2]^-$ and $[Eu\mathbf{3}_2]^-$. XTA solvent dependence plots and discussion. TD-DFT results and table of relevant parameters. $^5D_1$ emission lines for $[Eu\mathbf{1}_2]^-$, $[Eu\mathbf{2}_2]^-$, and $[Eu\mathbf{3}_2]^-$. Low-temperature ligand phosphorescence spectra. This material is available free of charge via the Internet at http://pubs.acs.org.

Acknowledgements

This material is based upon work supported by the U.S. Department of Energy, Office of Science, Office of Basic Energy Sciences, Separation Science program under Award Number DE-SC0016961. This research used resources of the Advanced Photon Source, a U.S. Department of Energy (DOE) Office of Science User Facility

operated for the DOE Office of Science by Argonne National Laboratory under Contract No. DE-AC02-06CH11357. Work by M.W.M. and K.N.R. was supported by the U.S. Department of Energy, Basic Energy Science under Contract No. DE-SC0016961. Work by A.M.M. and G.D. was supported by the U.S. Department of Energy, Office of Science, Basic Energy Science, Chemical Sciences, Geosciences and Biosciences Division under contract no. DE-AC02- 06CH11357. Partial financial support by the Australian Research Council (ARC-DP170101895) is gratefully acknowledged (E. G. M.). We thank Dr. Donald Walko for assistance in measurements performed at beamline 7-ID of the Advanced Photon Source.

References

1. Shur, M. S.; Zukauskas, R., Solid-State Lighting: Toward Superior Illumination. *Proceedings of the IEEE* **2005,** *93* (10), 1691-1703.
2. Gundiah, G.; Shimomura, Y.; Kijima, N.; Cheetham, A. K., Novel red phosphors based on vanadate garnets for solid state lighting applications. *Chemical Physics Letters* **2008,** *455* (4), 279-283.
3. Desurvire, E.; Simpson, J. R.; Becker, P. C., High-gain erbium-doped traveling-wave fiber amplifier. *Opt. Lett.* **1987,** *12* (11), 888-890.
4. Heer, S.; Lehmann, O.; Haase, M.; Güdel, H.-U., Blue, Green, and Red Upconversion Emission from Lanthanide-Doped LuPO4 and YbPO4 Nanocrystals in a Transparent Colloidal Solution. *Angewandte Chemie International Edition* **2003,** *42* (27), 3179-3182.
5. Steckl, A. J.; Zavada, J. M., Optoelectronic Properties and Applications of Rare-Earth-Doped GaN. *MRS Bulletin* **2013,** *24* (9), 33-38.
6. Pandya, S.; Yu, J.; Parker, D., Engineering emissive europium and terbium complexes for molecular imaging and sensing. *Dalton Transactions* **2006,** (23), 2757-2766.
7. Moore, E. G.; Samuel, A. P. S.; Raymond, K. N., From Antenna to Assay: Lessons Learned in Lanthanide Luminescence. *Accounts of Chemical Research* **2009,** *42* (4), 542-552.
8. Bünzli, J.-C. G., On the design of highly luminescent lanthanide complexes. *Coordination Chemistry Reviews* **2015,** *293-294*, 19-47.
9. Soini, E.; Hemmilä, I., Fluoroimmunoassay: present status and key problems. *Clinical Chemistry* **1979,** *25* (3), 353-361.
10. Soini, E.; Lövgren, T.; Reimer, C. B., Time-Resolved Fluorescence of Lanthanide Probes and Applications in Biotechnology. *C R C Critical Reviews in Analytical Chemistry* **1987,** *18* (2), 105-154.
11. Bünzli, J.-C. G., Lanthanide Luminescence for Biomedical Analyses and Imaging. *Chemical Reviews* **2010,** *110* (5), 2729-2755.
12. Bünzli, J.-C. G., Rising Stars in Science and Technology: Luminescent Lanthanide Materials. *European Journal of Inorganic Chemistry* **2017,** *2017* (44), 5058-5063.
13. Bünzli, J.-C. G.; Eliseeva, S. V., Lanthanide NIR luminescence for telecommunications, bioanalyses and solar energy conversion. *Journal of Rare Earths* **2010,** *28* (6), 824-842.
14. Bünzli, J.-C. G.; Eliseeva, S. V., Basics of Lanthanide Photophysics. In *Lanthanide Luminescence: Photophysical, Analytical and Biological Aspects*, Hänninen, P.; Härmä, H., Eds. Springer Berlin Heidelberg: Berlin, Heidelberg, 2011; pp 1-45.
15. Petoud, S.; Cohen, S. M.; Bünzli, J.-C. G.; Raymond, K. N., Stable Lanthanide Luminescence Agents Highly Emissive in Aqueous Solution: Multidentate 2-Hydroxyisophthalamide Complexes of Sm3+, Eu3+, Tb3+, Dy3+. *Journal of the American Chemical Society* **2003,** *125* (44), 13324-13325.
16. Soulié, M.; Latzko, F.; Bourrier, E.; Placide, V.; Butler, S. J.; Pal, R.; Walton, J. W.; Baldeck , P. L.; Le Guennic, B.; Andraud, C.; Zwier, J. M.; Lamarque, L.; Parker, D.; Maury, O., Comparative Analysis of Conjugated Alkynyl Chromophore–Triazacyclononane Ligands for Sensitized Emission of Europium and Terbium. *Chemistry – A European Journal* **2014,** *20* (28), 8636-8646.

17. Walton, J. W.; Bourdolle, A.; Butler, S. J.; Soulie, M.; Delbianco, M.; McMahon, B. K.; Pal, R.; Puschmann, H.; Zwier, J. M.; Lamarque, L.; Maury, O.; Andraud, C.; Parker, D., Very bright europium complexes that stain cellular mitochondria. *Chemical Communications* **2013,** *49* (16), 1600-1602.
18. Lazarides, T.; Adams, H.; Sykes, D.; Faulkner, S.; Calogero, G.; Ward, M. D., Heteronuclear bipyrimidine-bridged Ru–Ln and Os–Ln dyads: low-energy 3MLCT states as energy-donors to Yb(iii) and Nd(iii). *Dalton Transactions* **2008,** (5), 691-698.
19. Lazarides, T.; Davies, G. M.; Adams, H.; Sabatini, C.; Barigelletti, F.; Barbieri, A.; Pope, S. J. A.; Faulkner, S.; Ward, M. D., Ligand-field excited states of hexacyanochromate and hexacyanocobaltate as sensitisers for near-infrared luminescence from Nd(iii) and Yb(iii) in cyanide-bridged d–f assemblies. *Photochemical & Photobiological Sciences* **2007,** *6* (11), 1152-1157.
20. Lazarides, T.; Sykes, D.; Faulkner, S.; Barbieri, A.; Ward, M. D., On the Mechanism of d–f Energy Transfer in RuII/LnIII and OsII/LnIII Dyads: Dexter-Type Energy Transfer Over a Distance of 20 Å. *Chemistry – A European Journal* **2008,** *14* (30), 9389-9399.
21. Ward, M. D., Mechanisms of sensitization of lanthanide(III)-based luminescence in transition metal/lanthanide and anthracene/lanthanide dyads. *Coordination Chemistry Reviews* **2010,** *254* (21), 2634-2642.
22. Moore, E. G.; Xu, J.; Jocher, C. J.; Werner, E. J.; Raymond, K. N., "Cymothoe sangaris": An Extremely Stable and Highly Luminescent 1,2-Hydroxypyridinonate Chelate of Eu(III). *Journal of the American Chemical Society* **2006,** *128* (33), 10648-10649.
23. Moore, E. G.; Grilj, J.; Vauthey, E.; Ceroni, P., A comparison of sensitized Ln(iii) emission using pyridine- and pyrazine-2,6-dicarboxylates - part II. *Dalton Transactions* **2013,** *42* (6), 2075-2083.
24. Law, G.-L.; Pham, T. A.; Xu, J.; Raymond, K. N., A Single Sensitizer for the Excitation of Visible and NIR Lanthanide Emitters in Water with High Quantum Yields. *Angewandte Chemie International Edition* **2012,** *51* (10), 2371-2374.
25. Xu, J.; Corneillie, T. M.; Moore, E. G.; Law, G.-L.; Butlin, N. G.; Raymond, K. N., Octadentate Cages of Tb(III) 2-Hydroxyisophthalamides: A New Standard for Luminescent Lanthanide Labels. *Journal of the American Chemical Society* **2011,** *133* (49), 19900-19910.
26. Li, N.; Subramanian, G. S.; Matthews, P. D.; Xiao, J.; Chellappan, V.; Rosser, T. E.; Reisner, E.; Luo, H.-K.; Wright, D. S., Energy transfer and photoluminescence properties of lanthanide-containing polyoxotitanate cages coordinated by salicylate ligands. *Dalton Transactions* **2018,** *47* (16), 5679-5686.
27. Lehn, J.-M., Perspectives in Supramolecular Chemistry—From Molecular Recognition towards Molecular Information Processing and Self-Organization. *Angewandte Chemie International Edition in English* **1990,** *29* (11), 1304-1319.
28. Lis, S.; Elbanowski, M.; Mkowska, B.; Hnatejko, Z., Energy transfer in solution of lanthanide complexes. *Journal of Photochemistry and Photobiology A: Chemistry* **2002,** *150* (1), 233-247.
29. Lindén, S.; Singh, M. K.; Wegner, K. D.; Regairaz, M.; Dautry, F.; Treussart, F.; Hildebrandt, N., Terbium-based time-gated Förster resonance energy transfer imaging for evaluating protein–protein interactions on cell membranes. *Dalton Transactions* **2015,** *44* (11), 4994-5003.
30. Rajendran, M.; Miller, Lawrence W., Evaluating the Performance of Time-Gated Live-Cell Microscopy with Lanthanide Probes. *Biophysical Journal* **2015,** *109* (2), 240-248.
31. Martínez-Pinilla, E.; Rabal, O.; Reyes-Resina, I.; Zamarbide, M.; Navarro, G.; Sánchez-Arias, J. A.; de Miguel, I.; Lanciego, J. L.; Oyarzabal, J.; Franco, R., Two Affinity Sites of the Cannabinoid Subtype 2 Receptor Identified by a Novel Homogeneous Binding Assay. *Journal of Pharmacology and Experimental Therapeutics* **2016,** *358* (3), 580-587.
32. Ward, R. J.; Pediani, J. D.; Milligan, G., Ligand-induced internalization of the orexin OX1 and cannabinoid CB1 receptors assessed via N-terminal SNAP and CLIP-tagging. *British Journal of Pharmacology* **2011,** *162* (6), 1439-1452.

33. D'Aléo, A.; Moore, E. G.; Szigethy, G.; Xu, J.; Raymond, K. N., Aryl Bridged 1-Hydroxypyridin-2-one: Effect of the Bridge on the Eu(III) Sensitization Process. *Inorganic Chemistry* **2009,** *48* (19), 9316-9324.
34. Daumann, L. J.; Tatum, D. S.; Andolina, C. M.; Pacold, J. I.; D'Aléo, A.; Law, G.-l.; Xu, J.; Raymond, K. N., Effects of Ligand Geometry on the Photophysical Properties of Photoluminescent Eu(III) and Sm(III) 1-Hydroxypyridin-2-one Complexes in Aqueous Solution. *Inorganic Chemistry* **2016,** *55* (1), 114-124.
35. Daumann, L. J.; Tatum, D. S.; Snyder, B. E. R.; Ni, C.; Law, G.-l.; Solomon, E. I.; Raymond, K. N., New Insights into Structure and Luminescence of EuIII and SmIII Complexes of the 3,4,3-LI(1,2-HOPO) Ligand. *Journal of the American Chemical Society* **2015,** *137* (8), 2816-2819.
36. Moore, E. G.; Jocher, C. J.; Xu, J.; Werner, E. J.; Raymond, K. N., An Octadentate Luminescent Eu(III) 1,2-HOPO Chelate with Potent Aqueous Stability. *Inorganic Chemistry* **2007,** *46* (14), 5468-5470.
37. Moore, E. G.; Xu, J.; Jocher, C. J.; Castro-Rodriguez, I.; Raymond, K. N., Highly Luminescent Lanthanide Complexes of 1-Hydroxy-2-pyridinones. *Inorganic Chemistry* **2008,** *47* (8), 3105-3118.
38. Sá Ferreira, R. A.; Carlos, L. D.; Gonçalves, R. R.; Ribeiro, S. J. L.; de Zea Bermudez, V., Energy-Transfer Mechanisms and Emission Quantum Yields In Eu3+-Based Siloxane-Poly(oxyethylene) Nanohybrids. *Chemistry of Materials* **2001,** *13* (9), 2991-2998.
39. de Andrade, A. V. M.; da Costa, N. B.; Simas, A. M.; de Sá, G. F., Sparkle model for the quantum chemical AM1 calculation of europium complexes of coordination number nine. *Journal of Alloys and Compounds* **1995,** *225* (1), 55-59.
40. Jørgensen, C. K.; Judd, B. R., Hypersensitive pseudoquadrupole transitions in lanthanides. *Molecular Physics* **1964,** *8* (3), 281-290.
41. Judd, B. R., Optical Absorption Intensities of Rare-Earth Ions. *Physical Review* **1962,** *127* (3), 750-761.
42. Judd, B. R., Ionic transitions hypersensitive to environment. *The Journal of Chemical Physics* **1979,** *70* (11), 4830-4833.
43. Dutra, J. D. L.; Lima, N. B. D.; Freire, R. O.; Simas, A. M., Europium Luminescence: Electronic Densities and Superdelocalizabilities for a Unique Adjustment of Theoretical Intensity Parameters. *Scientific Reports* **2015,** *5*, 13695.
44. Lima, N. B. D.; Dutra, J. D. L.; Gonçalves, S. M. C.; Freire, R. O.; Simas, A. M., Chemical Partition of the Radiative Decay Rate of Luminescence of Europium Complexes. *Scientific Reports* **2016,** *6*, 21204.
45. Förster, T., Excitation transfer and internal conversion. *Chemical Physics Letters* **1971,** *12* (2), 422-424.
46. Dexter, D. L., A Theory of Sensitized Luminescence in Solids. *The Journal of Chemical Physics* **1953,** *21* (5), 836-850.
47. de Sá, G. F.; Malta, O. L.; de Mello Donegá, C.; Simas, A. M.; Longo, R. L.; Santa-Cruz, P. A.; da Silva, E. F., Spectroscopic properties and design of highly luminescent lanthanide coordination complexes. *Coordination Chemistry Reviews* **2000,** *196* (1), 165-195.
48. Hebbink, G. A.; Klink, S. I.; Grave, L.; Oude Alink, P. G. B.; van Veggel, F. C. J. M., Singlet Energy Transfer as the Main Pathway in the Sensitization of Near-Infrared Nd3+ Luminescence by Dansyl and Lissamine Dyes. *ChemPhysChem* **2002,** *3* (12), 1014-1018.
49. D'Aléo, A.; Picot, A.; Beeby, A.; Gareth Williams, J. A.; Le Guennic, B.; Andraud, C.; Maury, O., Efficient Sensitization of Europium, Ytterbium, and Neodymium Functionalized Tris-Dipicolinate Lanthanide Complexes through Tunable Charge-Transfer Excited States. *Inorganic Chemistry* **2008,** *47* (22), 10258-10268.
50. H. V. Werts, M.; A. Duin, M.; W. Hofstraat, J.; W. Verhoeven, J., Bathochromicity of Michler's ketone upon coordination with lanthanide(III) β-diketonates enables efficient sensitisation of Eu3+ for luminescence under visible light excitation†. *Chemical Communications* **1999,** (9), 799-800.
51. Vögtle, F.; Gorka, M.; Vicinelli, V.; Ceroni, P.; Maestri, M.; Balzani, V., A Dendritic Antenna for Near-Infrared Emission of Nd3+ Ions. *ChemPhysChem* **2001,** *2* (12), 769-773.
52. Klink, S. I.; Alink, P. O.; Grave, L.; Peters, F. G. A.; Hofstraat, J. W.; Geurts, F.; van Veggel, F. C. J. M., Fluorescent dyes as efficient photosensitizers for near-infrared Nd3+ emission. *Journal of the Chemical Society, Perkin Transactions 2* **2001,** (3), 363-372.

53. D'Aléo, A.; Pointillart, F.; Ouahab, L.; Andraud, C.; Maury, O., Charge transfer excited states sensitization of lanthanide emitting from the visible to the near-infra-red. *Coordination Chemistry Reviews* **2012,** *256* (15), 1604-1620.
54. D'Aléo, A.; Xu, J.; Moore, E. G.; Jocher, C. J.; Raymond, K. N., Aryl-Bridged 1-Hydroxypyridin-2-one: Sensitizer Ligands for Eu(III). *Inorganic Chemistry* **2008,** *47* (14), 6109-6111.
55. Yang, C.; Fu, L.-M.; Wang, Y.; Zhang, J.-P.; Wong, W.-T.; Ai, X.-C.; Qiao, Y.-F.; Zou, B.-S.; Gui, L.-L., A Highly Luminescent Europium Complex Showing Visible-Light-Sensitized Red Emission: Direct Observation of the Singlet Pathway. *Angewandte Chemie International Edition* **2004,** *43* (38), 5010-5013.
56. Kim, Y.; Son, Y.; Lee, J. In *Design Criteria of Transformer for LCD Backlight Inverter*, 2006 IEEE International Magnetics Conference (INTERMAG), 8-12 May 2006; 2006; pp 213-213.
57. Kadjane, P.; Charbonnière, L.; Camerel, F.; Lainé, P. P.; Ziessel, R., Improving Visible Light Sensitization of Luminescent Europium Complexes. *Journal of Fluorescence* **2008,** *18* (1), 119-129.
58. Shavaleev, N. M.; Scopelliti, R.; Gumy, F.; Bünzli, J.-C. G., Visible-Light Excitation of Infrared Lanthanide Luminescence via Intra-Ligand Charge-Transfer State in 1,3-Diketonates Containing Push-Pull Chromophores. *European Journal of Inorganic Chemistry* **2008,** *2008* (9), 1523-1529.
59. Archer, R. D.; Chen, H.; Thompson, L. C., Synthesis, Characterization, and Luminescence of Europium(III) Schiff Base Complexes1a. *Inorganic Chemistry* **1998,** *37* (8), 2089-2095.
60. Malta, O. L., Mechanisms of non-radiative energy transfer involving lanthanide ions revisited. *Journal of Non-Crystalline Solids* **2008,** *354* (42), 4770-4776.
61. Malta, O. L.; Brito, H. F.; Menezes, J. F. S.; Gonçalves e Silva, F. R.; de Mello Donegá, C.; Alves, S., Experimental and theoretical emission quantum yield in the compound Eu(thenoyltrifluoroacetonate)3.2(dibenzyl sulfoxide). *Chemical Physics Letters* **1998,** *282* (3), 233-238.
62. Malta, O. L.; Brito, H. F.; Menezes, J. F. S.; Silva, F. R. G. e.; Alves, S.; Farias, F. S.; de Andrade, A. V. M., Spectroscopic properties of a new light-converting device Eu(thenoyltrifluoroacetonate)3 2(dibenzyl sulfoxide). A theoretical analysis based on structural data obtained from a sparkle model. *Journal of Luminescence* **1997,** *75* (3), 255-268.
63. Faustino, W. M.; Nunes, L. A.; Terra, I. A. A.; Felinto, M. C. F. C.; Brito, H. F.; Malta, O. L., Measurement and model calculation of the temperature dependence of ligand-to-metal energy transfer rates in lanthanide complexes. *Journal of Luminescence* **2013,** *137*, 269-273.
64. Kasprzycka, E.; Trush, V. A.; Amirkhanov, V. M.; Jerzykiewicz, L.; Malta, O. L.; Legendziewicz, J.; Gawryszewska, P., Contribution of Energy Transfer from the Singlet State to the Sensitization of Eu3+ and Tb3+ Luminescence by Sulfonylamidophosphates. *Chemistry – A European Journal* **2017,** *23* (6), 1318-1330.
65. Alpha, B.; Ballardini, R.; Balzani, V.; Lehn, J.-M.; Perathoner, S.; Sabbatini, N., ANTENNA EFFECT IN LUMINESCENT LANTHANIDE CRYPTATES: A PHOTOPHYSICAL STUDY. *Photochemistry and Photobiology* **1990,** *52* (2), 299-306.
66. Chong, B. S. K.; Moore, E. G., Quantitative Sensitization Efficiencies in NIR-Emissive Homoleptic Ln(III) Complexes Using 2-(5-Methylpyridin-2-yl)-8-hydroxyquinoline. *Inorganic Chemistry* **2018,** *57* (22), 14062-14072.
67. Andres, J.; Chauvin, A.-S., Energy transfer in coumarin-sensitised lanthanide luminescence: investigation of the nature of the sensitiser and its distance to the lanthanide ion. *Physical Chemistry Chemical Physics* **2013,** *15* (38), 15981-15994.
68. Pacold, J. I.; Tatum, D. S.; Seidler, G. T.; Raymond, K. N.; Zhang, X.; Stickrath, A. B.; Mortensen, D. R., Direct Observation of 4f Intrashell Excitation in Luminescent Eu Complexes by Time-Resolved X-ray Absorption Near Edge Spectroscopy. *Journal of the American Chemical Society* **2014,** *136* (11), 4186-4191.
69. Werts, M. H. V.; Jukes, R. T. F.; Verhoeven, J. W., The emission spectrum and the radiative lifetime of Eu3+ in luminescent lanthanide complexes. *Physical Chemistry Chemical Physics* **2002,** *4* (9), 1542-1548.
70. Werts, M. H. V., Making sense of lanthanide luminescence. *Science Progress* **2005,** *88* (2), 101-131.

71. Snellenburg, J. J.; Laptenok, S.; Seger, R.; Mullen, K. M.; van Stokkum, I. H. M., Glotaran: A Java-Based Graphical User Interface for the R Package TIMP. *2012* **2012,** *49* (3), 22.
72. Walko, D. A.; Adams, B. W.; Doumy, G.; Dufresne, E. M.; Li, Y.; March, A. M.; Sandy, A. R.; Wang, J.; Wen, H.; Zhu, Y., Developments in time-resolved x-ray research at APS beamline 7ID. *AIP Conference Proceedings* **2016,** *1741* (1), 030048.
73. March, A. M.; Stickrath, A.; Doumy, G.; Kanter, E. P.; Krässig, B.; Southworth, S. H.; Attenkofer, K.; Kurtz, C. A.; Chen, L. X.; Young, L., Development of high-repetition-rate laser pump/x-ray probe methodologies for synchrotron facilities. *Review of Scientific Instruments* **2011,** *82* (7), 073110.
74. Khalil, M.; Marcus, M. A.; Smeigh, A. L.; McCusker, J. K.; Chong, H. H. W.; Schoenlein, R. W., Picosecond X-ray Absorption Spectroscopy of a Photoinduced Iron(II) Spin Crossover Reaction in Solution. *The Journal of Physical Chemistry A* **2006,** *110* (1), 38-44.
75. Holz, R. C.; Chang, C. A.; Horrocks, W. D., Spectroscopic characterization of the europium(III) complexes of a series of N,N'-bis(carboxymethyl) macrocyclic ether bis(lactones). *Inorganic Chemistry* **1991,** *30* (17), 3270-3275.
76. Baker, M. L.; Mara, M. W.; Yan, J. J.; Hodgson, K. O.; Hedman, B.; Solomon, E. I., K- and L-edge X-ray absorption spectroscopy (XAS) and resonant inelastic X-ray scattering (RIXS) determination of differential orbital covalency (DOC) of transition metal sites. *Coordination Chemistry Reviews* **2017,** *345*, 182-208.
77. DeBeer George, S.; Brant, P.; Solomon, E. I., Metal and Ligand K-Edge XAS of Organotitanium Complexes: Metal 4p and 3d Contributions to Pre-edge Intensity and Their Contributions to Bonding. *Journal of the American Chemical Society* **2005,** *127* (2), 667-674.
78. Westre, T. E.; Kennepohl, P.; DeWitt, J. G.; Hedman, B.; Hodgson, K. O.; Solomon, E. I., A Multiplet Analysis of Fe K-Edge 1s → 3d Pre-Edge Features of Iron Complexes. *Journal of the American Chemical Society* **1997,** *119* (27), 6297-6314.
79. Beeby, A.; Faulkner, S.; Parker, D.; Williams, J. A. G., Sensitised luminescence from phenanthridine appended lanthanide complexes: analysis of triplet mediated energy transfer processes in terbium, europium and neodymium complexes. *Journal of the Chemical Society, Perkin Transactions 2* **2001,** (8), 1268-1273.
80. Beeby, A.; Bushby, L. M.; Maffeo, D.; Williams, J. A. G., The efficient intramolecular sensitisation of terbium(III) and europium(III) by benzophenone-containing ligands. *Journal of the Chemical Society, Perkin Transactions 2* **2000,** (7), 1281-1283.
81. Zhang, Q.; Wu, L.; Cao, X.; Chen, X.; Fang, W.; Dolg, M., Energy Resonance Crossing Controls the Photoluminescence of Europium Antenna Probes. *Angewandte Chemie International Edition* **2017,** *56* (27), 7986-7990.

Tables

Table 1: Luminescence Properties of Eu(III) Complexes in Methanol			
Complex	$[Eu\mathbf{1}_2]^-$	$[Eu\mathbf{2}_2]^-$	$[Eu\mathbf{3}_2]^-$
λ_{max} (nm)	338	341	347
τ_{obs} MeOH (μs)	788	758	651
τ_{obs} d_4-MeOH (μs)	960	912	765
m (# bound MeOH)	0.48	0.47	0.48
Φ_{tot} MeOH	0.30	0.30	0.11
Φ_{tot} d_4-MeOH	0.33	0.33	0.14
k_{rad} MeOH (s^{-1})	662	644	790
k_{nr} MeOH (s^{-1})	608	676	747
Φ_{Eu} MeOH	0.52	0.49	0.51
η_{sens} MeOH	0.57	0.61	0.21

Table 2: Optical Transient Absorption Fitting Results					
Complex	Metal	τ_1 (ps)	τ_2 (ps)	τ_3 (ns)	η_{ET}
$[M\mathbf{1}_2]^-$	Gd	10.6 ± 0.039	-	205.1 ± 0.76	0.995
	Eu	2.9 ± 0.018	-	1.1 ± 0.0029	
$[M\mathbf{2}_2]^-$	Gd	13.6 ± 0.043	-	157.3 ± 4.4	0.991
	Eu	2.3 ± 0.012	-	1.4 ± 0.0029	
$[M\mathbf{3}_2]^-$	Gd	1.9 ± 0.0040	8.8 ± 0.042	186.0 ± 1.6	0.991
	Eu	1.6 ± 0.0028	7.6 ± 0.030	1.7 ± 0.0050	

Figures

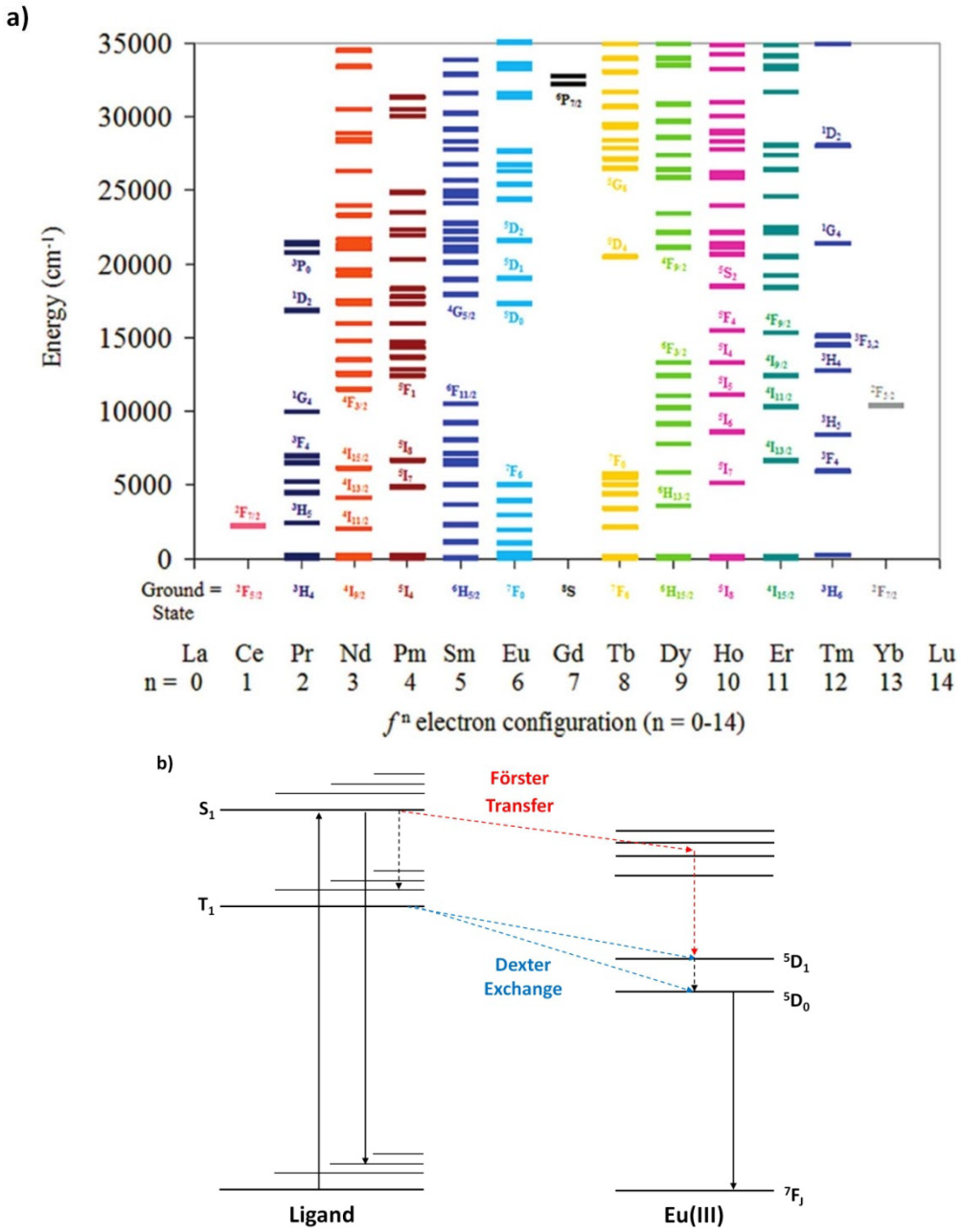

Figure 1: a) Energies of trivalent lanthanide 4f excited states;[7] b) Jablonski diagram of the ligand and lanthanide center dynamics following photoexcitation; Förster (red) and Dexter (blue) energy transfer pathways are also shown. Note that at higher temperatures, the $^5D_0$ becomes available for Dexter charge exchange from the thermally-populated $^7F_1$

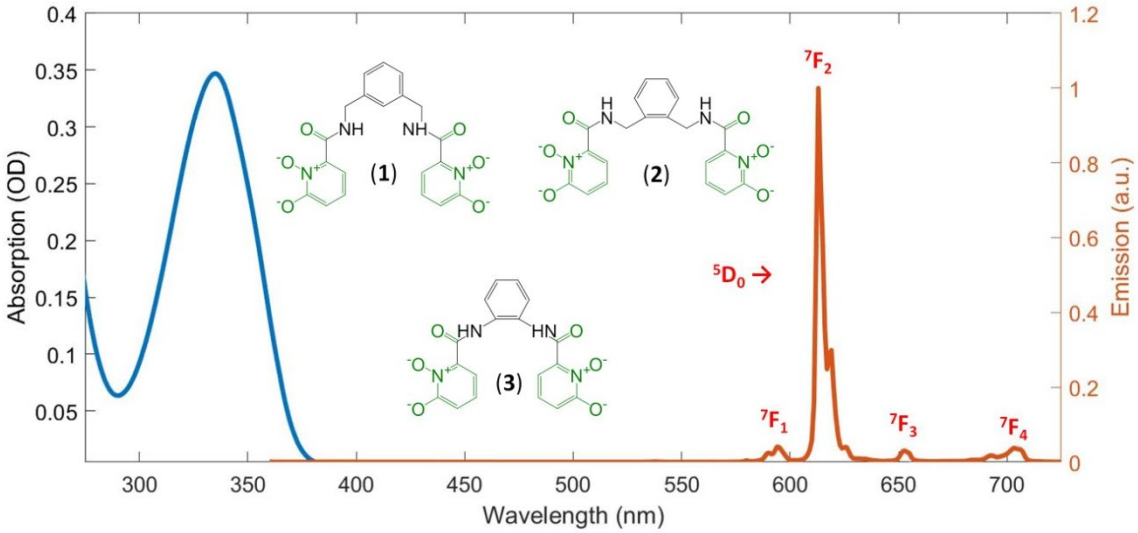

Figure 2: UV-Vis absorption (blue) and emission (red) spectrum for **1**. The most relevant Eu(III) emission lines are labeled. Ligand and molecular structures are shown in the middle

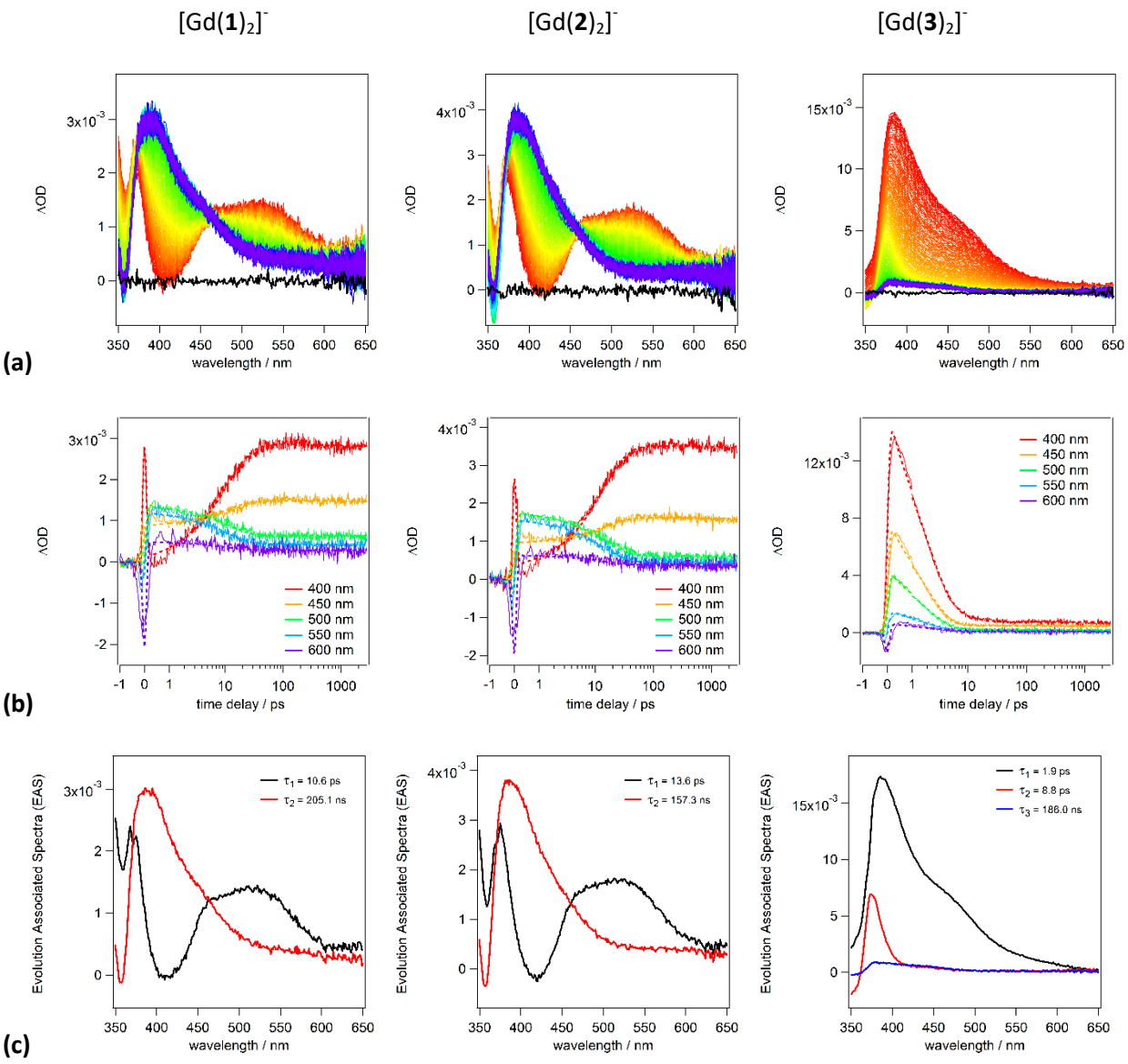

Figure 3: (a) Observed optical transient absorption spectra, (b) decay kinetics and global fits at selected wavelengths and (c) corresponding Evolution Associated Spectra for the [Gd**1**$_2$]$^-$ (left), [Gd**2**$_2$]$^-$ (middle), and [Gd**3**$_2$]$^-$ (right) complexes. The long time constant for each spectra was determined independently by nanosecond measurements (Supporting Information) and was fixed in the analysis.

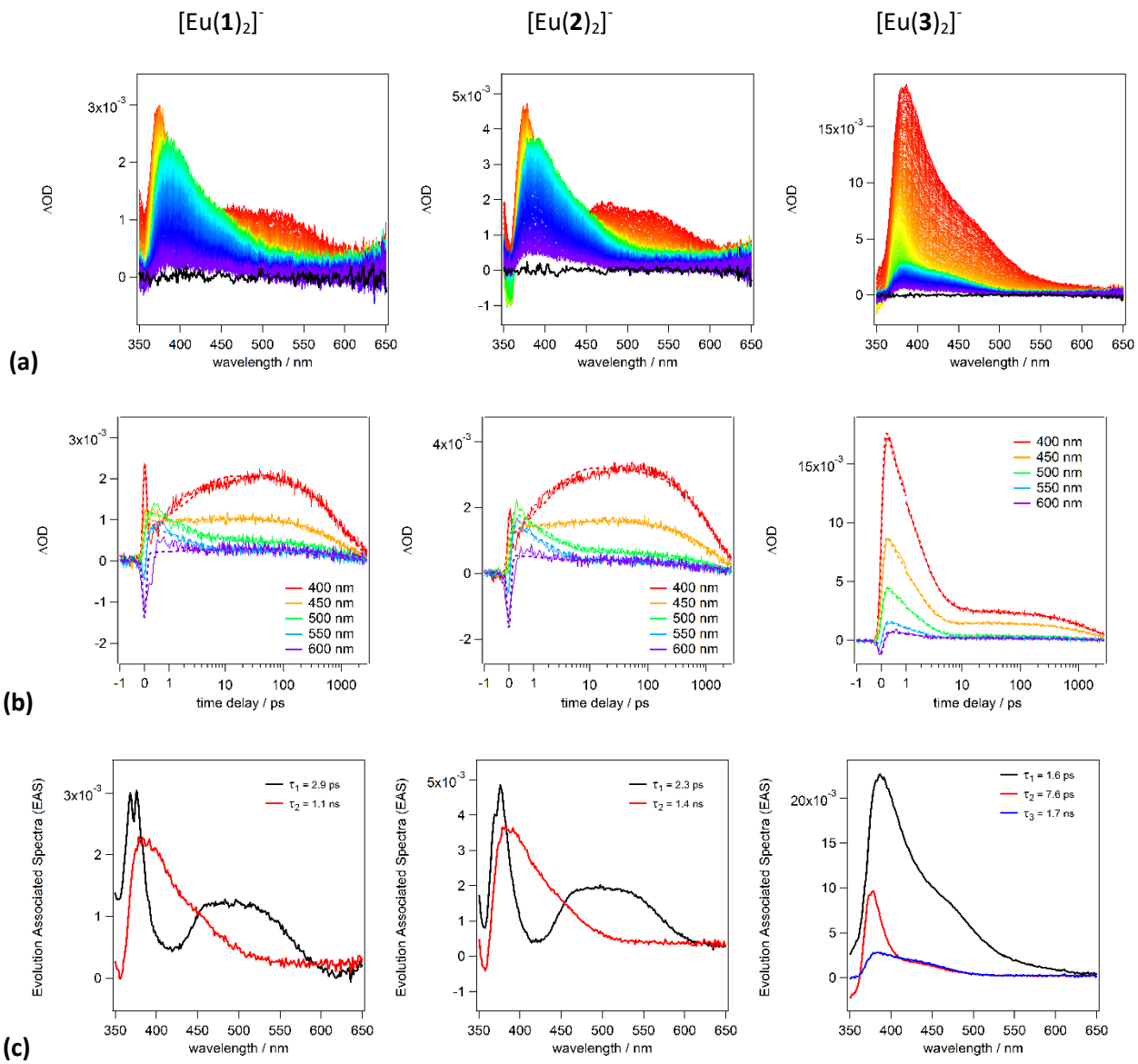

Figure 4: (a) Observed optical transient absorption spectra, (b) decay kinetics and global fits at selected wavelengths and (c) corresponding Evolution Associated Spectra for the [Eu**1**$_2$]$^-$ (left), [Eu**2**$_2$]$^-$ (middle), and [Eu**3**$_2$]$^-$ (right) complexes.

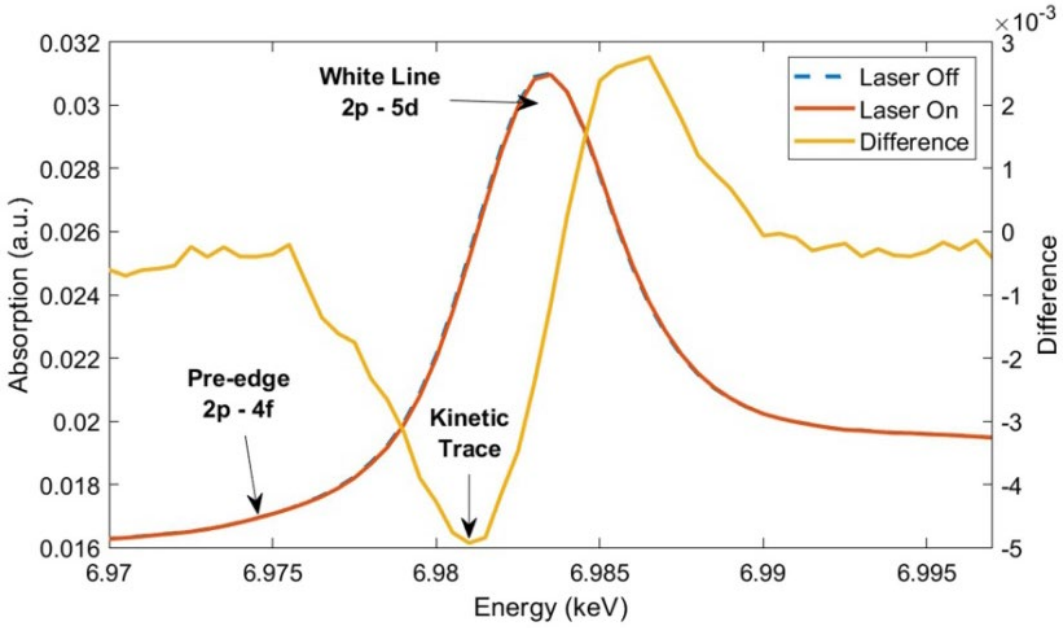

Figure 5: Ground-state (blue dashed) and laser-excited (red, 5 ns delay) Eu L3-edge X-ray absorption spectra of $[Eu\mathbf{2}_2]^-$. The laser on – laser off difference spectra (yellow) is plotted on the right y-axis

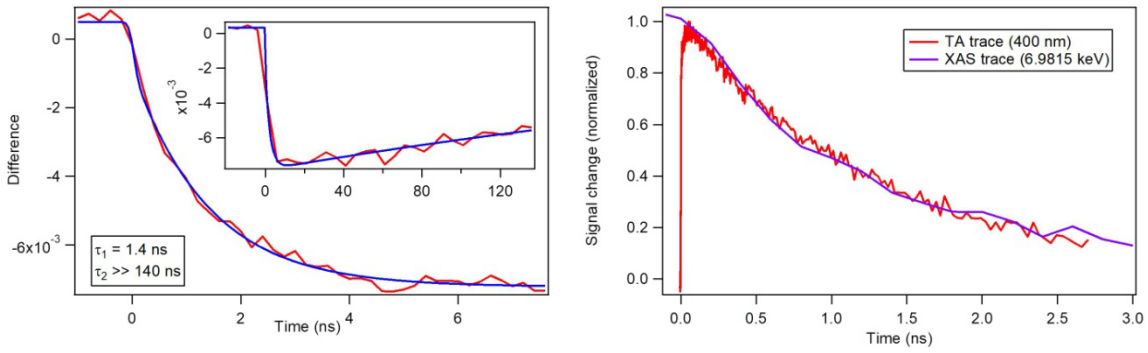

Figure 6: Left: Temporal dynamics of Eu L3 X-ray absorption spectrum of $[Eu\mathbf{2}_2]^-$, collected at 6.9815 keV. Right: Comparison of normalized X-ray trace (blue) with optical transient absorption trace (red) at 400 nm

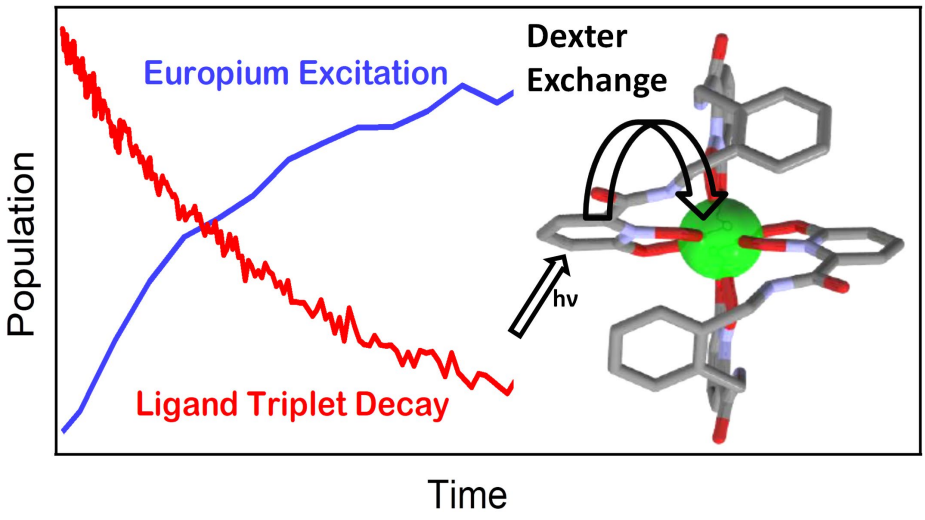
Europium Excitation
Dexter
Exchange
Ligand Triplet Decay
hv
Population
Time

TOC Image